Solvent-assisted morphology confinement of a nickel sulfide nanostructure and its application for non-enzymatic glucose sensor

Soochan Kim, Sang Ha Lee, Misuk Cho, Youngkwan Lee

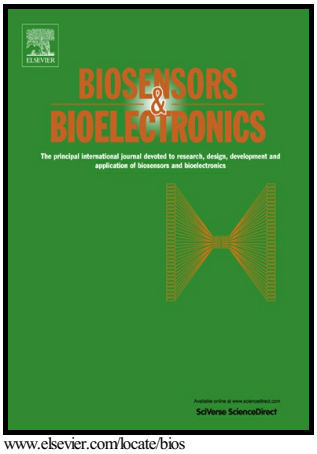

www.elsevier.com/locate/bios

PII: S0956-5663(16)30493-6
DOI: http://dx.doi.org/10.1016/j.bios.2016.05.062
Reference: BIOS8752

To appear in: *Biosensors and Bioelectronic*

Received date: 1 April 2016
Revised date: 11 May 2016
Accepted date: 20 May 2016

Cite this article as: Soochan Kim, Sang Ha Lee, Misuk Cho and Youngkwai Lee, Solvent-assisted morphology confinement of a nickel sulfide nanostructur and its application for non-enzymatic glucose sensor, *Biosensors an Bioelectronic,* http://dx.doi.org/10.1016/j.bios.2016.05.062

Solvent-assisted morphology confinement of a nickel sulfide nanostructure and its application for non-enzymatic glucose sensor

Soochan Kim, Sang Ha Lee, Misuk Cho, Youngkwan Lee[*]

School of Chemical Engineering, Sungkyunkwan University, Suwon 440-746, Republic of Korea

[*]Corresponding author: Tel. +82-31-290-7248. Fax: +82-31-290-7272. yklee@skku.edu

Abstract

Morphology-controlled synthesis of nickel sulfide (Ni_3S_2) was performed directly on Ni foam using thioacetamide as a sulfur ion source. Various morphologies of nickel sulfide were fabricated using a hydrothermal process by adjusting the solvent composition of ethanol and water. In the water-dominant condition, a dendrite structure was obtained; otherwise, a flaky structure was achieved. A hierarchical cauliflower-like structure was obtained at a solvent mixture composition of 1:1 and was used as non-enzymatic glucose sensor. The hierarchical Ni_3S_2 electrode showed a high level of electro-catalytic activity toward the oxidation of glucose (16,460 $\mu AmM^{-1}cm^{-2}$) over a wide range of detection (0.0005 – 3 mM) and a low detection limit (0.82 μM) with excellent selectivity in the presence of several electroactive species.

Key words: nickel sulfide, hierarchical cauliflower, solvent assist, glucose, biosensor

1. Introduction

Diabetes is one of the most serious diseases threatening human health. The diagnosis and management of diabetes mellitus require quick and accurate testing of blood glucose level (Yang et al., 2013; Shen et al., 2007; Huo et al., 2014). Conventional glucose sensors are based on the enzymatic method. These enzymatic-type sensors suffer from instable enzyme activity due to the immobilization process and storage period, which are significant

problems with most sensor designs (Zhao et al., 2015). Therefore, non-enzymatic sensors based on the electrochemical method have received increasing interest in recent years. Electrochemical glucose sensors can provide better analytical characteristics in terms of selectivity, sensitivity, reliability, and ease of fabrications and use (Wang et al. 2008; Bojdi et al., 2014; Hosseini et al., 2014;).

Of the various active materials used in non-enzymatic sensors, metal chalcogenides have gained prominence due to their distinct physical and chemical properties (Ghosh et al., 2015). Many researchers have designed non-enzymatic glucose sensors based on metal oxide due to their abundance and low cost compared to other materials such as noble and noble alloy metals (Wang et al., 2009; Cao et al., 2011). Metal sulfides also have catalytic activity, a rich reserve, and low cost similar to that of metal oxides. However, the electrochemical investigation of metal sulfides remains in preliminary stages and requires attention due to the overall rich redox chemistry, improved electrical conductivity, mechanical properties, and thermal stability compared to those of corresponding metal oxides and selenides (Zhao et al., 2015; Lee et al., 2015a; Jung et al., 2014). Studies on metal sulfides have focused on their electrochemical applications: copper sulfide in non-enzymatic glucose sensors (Qian et al., 2013), iron sulfide in the detection of hydrogen peroxide (Lee et al., 2015b), nickel sulfide and cobalt sulfide for dye-sensitized solar cells (Zhang et al., 2008), and molybdenum sulfide as a catalyst of hydrogen evolution (Li et al., 2014).

Nickel sulfide (Ni_3S_2) is a metallic conductor with a resistivity as low as 1.8×10^{-5} Ω at room temperature (Metcalf et al., 1993). Ni_3S_2, present in various morphologies and nanostructures, has been investigated in the application of supercapacitors, catalysts, and electrochemical sensors (Huo et al., 2014; Chou et al., 2013; Zhang et al., 2014; Zhou et al.,

2013). To alleviate the conductivity of Ni_3S_2, Ni-foam has been utilized as a three-dimensional substance to obtain more exposed surface area and faster electron transfer. Previous reports have studied the connection of Ni_3S_2 and Ni-foam. Three-dimensional Ni_3S_2 nanosheet arrays for supercapacitors and non-enzymatic glucose sensor applications were hydrothermally synthesized on Ni foam using nickel nitrate and thiourea (Huo et al., 2014). A flaky Ni_3S_2 nanostructure was electrochemically deposited on Ni foam using nickel chloride and thiourea in order to form supercapacitors (Chou et al., 2013). In this case, the active material, Ni_3S_2, easily flaked and fell off of the Ni-foam.

The other strategy is directly growing Ni_3S_2 on Ni-foam as reactant and substrate. The dendrite structure of Ni_3S_2 on Ni foam as a reactive substrate using thioacetamide was prepared by adjusting the reaction temperature (120 - 180˚C) and time (2 - 8h) in water for use in supercapacitors (Zhang et al., 2014). Ni_3S_2 nanorods on Ni foam using thioacetamide were also prepared by adjusting the reaction time (2 - 6h) at 180˚C in water for electro-catalytic oxygen evolution (Zhou et al., 2013). According to these studies, the morphology of nickel sulfide was controlled by changing the temperature and time; however, no significant change in morphology was demonstrated. Morphology control might also be possible through the use of different precursors (Yu et al., 2002), additives (Zhang et al., 2004), or templates (Wang et al., 2006b), which make the synthesis process more complex. Therefore, a controlled process of formation of nanostructured Ni_3S_2 on Ni foam would be remarkable for practical applications.

Herein, we designed Ni_3S_2 with various morphologies on Ni foam by simply adjusting the solvent composition. Generally, the polarity and coordination of the reaction medium have great influence on the reactivity and diffusion of reactants. Ultimately, these factors influence the structure and morphological features of the resulting products. However,

studies on the solvent-assisted morphology confinement of Ni_3S_2 structure have not been reported. Various morphologies of Ni_3S_2 were directly prepared on Ni foam using a simple hydrothermal method in an eco-friendly environment of ethanol and water. A hierarchical structure of Ni_3S_2 was obtained by controlling the reaction medium, and the electrochemical properties were confirmed as a function of the morphology. The prepared hierarchical Ni_3S_2 electrode was applied to detect glucose, exhibiting very high sensitivity, good selectivity, and repeatability.

2. Experimental Section

2.1 Materials

All reagents were analytical grade and were used as received without further purification. Ni foam was purchased from Wellcos Co., Ltd. (Gunpo, Republic of Korea). Thioacetamide (TAA), glucose, fructose, lactose, ascorbic acid (AA), uric acid (UA), and dopamine (DA) were purchased from Sigma-Aldrich (Saint Louis, MO, USA). Deionized water and absolute ethanol were supplied by Duksan Co., Ltd. (Ansan, Republic of Korea). A 0.5 M NaOH solution was purchased from Samchun Co., Ltd. (Pyeoungtaek, Republic of Korea).

2.2 Preparation of nickel sulfide on Ni foam

Nickel sulfide was prepared on a piece of Ni foam (1 x 1 cm) using a hydrothermal process. The Ni foam was successively purified in acetone, 3 M HCl, deionized water, and absolute ethanol under ultra-sonication and then dried in a vacuum oven for 2h. The foam was then transferred to a Teflon-lined stainless steel autoclave filled with TAA (0.017 M) and ethanol and/or water. The sealed autoclave was heated in an oven at 120 °C for 6h. After the autoclave was cooled to room temperature, the product was washed with ethanol and

deionized water and then dried in a vacuum at 60 °C for 8h. As a result, nickel sulfide electrodes were prepared with various morphologies by changing the reaction conditions. The reaction temperature and time ranges were verified at 90 - 160 °C and 3 - 12h, respectively. Nickel sulfides were not formed in ethanol or water at 90 °C for 12h. At 160 °C for 3h, a nickel sulfide cluster was formed in ethanol and water. Thus, the reaction temperature and time were set at 120 °C for 6h. The volume ratio between ethanol and water was set to 1:0, 2:1, 1:1, 1:2, or 0:1.

2.3 Characterization

The surface morphology of the nickel sulfide was observed by scanning electron microscopy (SEM, JEOL JSM-7000F, and Japan). X-ray diffraction (XRD) patterns were collected using a Bruker D8 Advance diffractometer (Germany) equipped with a Cu Kα source (λ = 1.54056 Å). X-ray photoelectron spectroscopy (XPS) was performed using a VG Scientific ESCA 2000 spectrometer with an Al-K^{α} X-ray source operating at a power of 170W (13 mA and 13 kV).

2.4 Electrochemical measurements

Electrochemical measurements of the prepared nickel sulfide were performed in a three-electrode system. Nickel sulfide on Ni foam, a platinum electrode, and Ag/AgCl (sat'd KCl solution) were used as the working, counter, and reference electrodes, respectively. A solution of 0.5 M NaOH was used as the electrolyte. Cyclic voltammetry (CV), chronoamperometry (CA), and electrochemical impedance spectroscopy (EIS) measurements were performed on a VSP potentiostat (Princeton Applied Research, USA) at room temperature. At least 5 test samples were measured to obtain the average and relative

standard deviations (RSD).

3. Results and Discussion

3.1 Morphology and composition of nickel sulfide

The preparation of nickel sulfide on the Ni foam is schematically represented in Figure 1. In the reaction, TAA was needed to supply sulfur ions to react with the surface of the Ni foam, and nickel sulfides were obtained directly on the Ni foam (Wang et al., 2014). The result was a three-dimensional porous structure of the Ni foam in which the diameter of the pore was approximately 100 - 200 μm. The porous structure provides easy ion diffusion and electron transfer. Ni_3S_2 crystals with the desired morphology can be obtained by control of the solvent composition of ethanol and water. In ethanol medium, flake structures with nanowalls of Ni_3S_2 crystals were obtained and changed into dendrites with the addition of water.

Various morphologies of Ni_3S_2 according to the ratio of ethanol to water are shown in Figures 2 and S1 (see Supporting Information). Figure 2A shows the Ni_3S_2 flakes formed in ethanol. When a small amount of water was added, the flakes started to coagulate, and larger particles were formed, as shown in Figures S1 (B)-(C). In the case of the mixed solvent system of ethanol and water (1/1, v/v) shown in Figure 2B, a cauliflower-like structure was observed. As shown in the high magnification images in Figure 2C, aggregated flakes were observed, indicating that a hierarchical structure can be produced. By increasing the water content, the cauliflower-like structures gradually transformed to dendritic structures, as shown in Figures S1 (E)-(F). The SEM image in Figure 2D presents a dendritic morphology in which the sizes of the trunk and branches were 10 - 30 and 0.5 - 5 μm, respectively. The growth was initiated from the center of the crystals and extended outward to form the trunks

and the branches of the dendrites. Additionally, the dendrite structures grew from the crystal center through a diffusion-limited process. In addition, EDS analysis and elemental mapping confirmed that the cauliflower-like structures consisted of Ni, S, and O (Figures 2E and S2). The O present was likely due to traces of oxide. As shown in the analysis, Ni and S elements were homogeneously distributed throughout the formed structure.

Considering that all of the nickel sulfides were synthesized at the same temperature and time, the resulting varied morphologies should be dependent on the reaction solvents in the hydrothermal synthesis. The polarity and coordinating ability of the mixed medium have strong effects on the reactivity, saturated vapor pressure, dielectric constant, and diffusion behavior of the reactants (Wang et al., 2006a). Thus, the solvent composition ultimately influences the morphological features of the resulting products.

According to the experimental results, the solvent composition has a significant influence on the final morphology and structure of the Ni_3S_2 crystals. With respect to the polarity of the solvent, water has a relatively high polarity compared to ethanol. In the hydrothermal treatment, water is in a state of lower saturated vapor pressure than ethanol. With a decrease in water content, the polarity of the solution decreases; thus, the reactivity of the reactant and the rate of nucleation of the crystal increase, which results in the formation of particles or flakes (Zhang et al., 2002; Cong et al., 2009). Compared to ethanol, a water molecule is quite small and can be easily polarized to effectively stabilize ions in the solution. Due to the high polarity of water and low reactivity of the reactant, water is liable to form a fractal pattern, such as flower-like structure or a dendrite, through a diffusion-limited process.

The crystalline nature of the phase and the surface elements of the nickel sulfides prepared in various media were determined via XRD, and the results are shown in Figures 3A and 3B. In Figure 3A, several well-defined diffraction peaks indicate that the obtained products were

well crystallized. All of the products in Figure 3 exhibited similar behavior and were considered to consist of Ni_3S_2. The peak intensity of Ni_3S_2-Et/W was greater than that for Ni_3S_2-Et or Ni_3S_2-W, indicating that Ni_3S_2-Et/W has an impressive crystallinity. The diffraction peaks were assigned by analyzing the image in Figure 3B. The notable peaks were located at 21.7°, 31.1°, 37.8°, 44.3°, 49.7°, 54.6°, 55.1°, 69.0°, 73.0°, and 77.9° and were respectively assigned to the (101), (110), (003), (202), (113), (104), (122), (303), (214), and (401) facets of hexagonal Ni_3S_2 with lattice constants of a = 5.745 Å and c =7.135 Å, which correspond to those in JCPDS No. 44-1418 (Huo et al., 2014; Zhou et al., 2010).

Detailed nickel sulfide phase information was also obtained from XPS. The spectrum (Figure 3) indicates the presence of Ni and S. The two strong peaks near 855.2 and 872.7 eV in Figure 3D can be attributed to Ni $2p_{3/2}$ and Ni $2p_{1/2}$, respectively. The peak at 852.7 eV is known as the characteristic peak of Ni_3S_2. The peak at 162.5 eV in Figure 3E can be assigned to S 2p. These results are in good agreement with the results reported in the literature (Wang et al., 2007; Zhou et al., 2013).

3.2 Electrochemical behavior of nickel sulfides

The electrochemical properties of the nickel sulfides were investigated by conducting electrochemical impedance (EIS) measurements and cyclic voltammetry (CV).

Figure 4A presents typical Nyquist plots obtained on four different electrodes. In the equivalent circuit from the inset of Figure 4A, R_s, W, R_{et}, and C represent the solution resistance, Warburg diffusion resistance, electron-transfer resistance, and double layer capacitance, respectively. The semicircle in the high-frequency range can be attributed to the resistance capacitance, e.g., electron-transfer process (Jung et al., 2014; Chou et al., 2008). ZSimpWin software was used to perform measurements according to the equivalent circuit

model. There was a small semicircle domain on the bare Ni foam (NF), implying a very low R_{et} with respect to the redox-probe dissolved in the solution. The bare NF exhibited a small electron transfer resistance of approximately 7.03 Ω cm^{-2}. The diameter of the Nyquist plot's semicircle changed upon reaction with TAA on the surface of NF and the production of nickel sulfides. The nickel sulfide prepared in ethanol, Ni_3S_2-Et, exhibited a R_{et} value of 14.60 Ω cm^{-2} (curve b). In the case of Ni_3S_2-Et/W (curve c), the diameter of the Nyquist plot semicircle decreased, which equates to a large reduction in R_{et} (R_{et} = 9.13 Ω cm^{-2}). The nickel sulfide prepared in water, Ni_3S_2-Et/W, exhibits a R_{et} value of 11.06 Ω cm^{-2} (curve d), which is smaller than those of the other electrodes. The difference in R_{et} was approximately 2 - 6 Ωcm^{-2}, and the result tended to change according to the morphology. As shown in Figure 2, Ni_3S_2-Et/W was expected to have a large surface area.

EIS is currently used as a non-destructive technique to provide useful information about the electrode surface. The electroactive surface area of the modified electrodes was also estimated by EIS, as in the literature (Chou et al., 2008; Lee et al., 2013). The electrochemically active specific surface (S_A) can be calculated from the specific capacitance of the electrochemical double layer with a constant value of 20 μFcm^{-2} (Chou et al., 2008). The electroactive surface area calculated for each electrode was 1.58 m^2g^{-1} for Ni_3S_2-Et/W, 0.13 m^2g^{-1} for Ni_3S_2-Et, and 0.97 m^2g^{-1} for Ni_3S_2W. The results of EIS are summarized in Table S1. The SEM images and EIS analysis were used to determine that the Ni_3S_2-Et/W has a porous open void structure, large electroactive surface area, and low electron transfer resistance compared to other Ni_3S_2 electrodes. The open void space in the hierarchical structure can serve as an "ion and electrolyte reservoir" to facilitate the transportation of electrolyte ions (Wang et al., 2006b). Based on the EIS analysis and SEM images, we conclude that the Ni_3S_2-Et/W exhibits the best electrochemical behavior among

the prepared nickel sulfide electrodes. In the present work, the electrochemical performance of nickel sulfide electrodes prepared under different medium conditions was measured by cyclic voltammetry.

Figure 4B shows cyclic voltammograms (CVs) of various nickel sulfide electrodes. The electrochemical reaction corresponding to the exhibited redox peaks is expressed as follows (Chou et al., 2015; Lin et al., 2014a):

$$Ni_3S_2 + OH^- \rightarrow Ni_3S_2OH + e^-$$

The oxidation and reduction peaks of CVs are located near 0.6 V and 0.35 V, respectively, within the potential range of 0 - 0.8 V and can be attributed to the reversible redox reaction of Ni^{2+}/Ni^{3+} and OH^- in an alkaline electrolyte. The result is consistent with the literature (Huo et al., 2014; Chou et al., 2013). The CV of the Ni_3S_2-Et/W electrode possesses a pair of broad redox peaks, a high current density, and a larger area under the CV compared to those of bare NF, Ni_3S_2-Et and Ni_3S_2-W. This is in good accord with the EIS results.

Figure 4C shows the CVs of the Ni_3S_2-Et/W electrode at different scan rates from 5 mVs^{-1} to 100 mVs^{-1}. With an increase in scan rate, the current response increases accordingly, and the peak shapes are well retained even at 100 mVs^{-1}, implying fast charge/discharge properties. The oxidation peak moved slightly toward the positive direction, and the reduction peak moved to the negative potential as the scan rate increased. The potential change might be caused by the strengthened electric polarization generated during the oxidation-reduction process. Figure 4D shows a good linear relationship between the redox peak current and the square root of the scanning rate $\nu^{1/2}$ with error bars: R^2 of oxidation peak current is 0.999 and R^2 of reduction peak current is 0.999. The electrochemical activity

on the electrode is controlled via diffusion, and the rates of electronic and ionic transfer in the electrode are sufficiently fast (Guo et al., 2014; Yang et al., 2016).

To evaluate the properties of the Ni_3S_2-Et/W electrode as a glucose sensor, the CV was measured in a 1 mM glucose solution. The oxidation peak current obviously increased when glucose was added to the NaOH solution. The Ni_3S_2-Et/W electrode exhibits the catalytic effect of the redox couple for the oxidation of glucose to gluconolactone:

$$Ni^{3+} + \text{glucose} + e^- \rightarrow Ni^{2+} + \text{gluconolactone}$$

The Ni^{3+} on the electrode surface rapidly oxidizes glucose at the anode, producing Ni^{2+} and sacrificing Ni^{3+}. This results in changes in the concentrations of Ni^{3+} and Ni^{2+} that cause an increase in the anodic peak current at +0.6 V (Huo et al., 2014; Chou et al., 2013).

3.3 Sensing characterization of the nickel sulfide electrode

The performance of the nickel sulfide electrodes to detect glucose was evaluated by chronoamperometry according to detection range, selectivity, reproducibility, and stability. The amperometric response was evaluated for the prepared electrode with successive addition of 0.1 mM glucose under different potentials from 0.5 V to 0.65 V (shown in Figure S3). At a potential of 0.55 V, the most significant increase in current was observed; thus, +0.55 V was chosen as the optimum working potential (Lu et al., 2015).

Figure 5 shows the amperometric responses of bare NF, Ni_3S_2–Et, Ni_3S_2–Et/W, and Ni_3S_2–

W electrodes with various morphologies at successive addition of glucose. A remarkable increase and fast response of amperometric current were observed with Ni_3S_2–Et/W, which has a hierarchical structure and large electroactive surface area, as shown by SEM and EIS analyses. The calibration curves of the prepared electrodes are plotted in Figure 5B. The increase in current density (μAcm^{-2}) was proportional to the glucose concentration (mM). It can be expressed in a model such as $y(\mu Acm^{-2}) = ax(mM) + b$, where a is the slope of the calibration curve as a sensitivity and R^2 is the coefficient of determination. The linear regression equations are: $y=1.148(\pm 0.24)\ x+0.2403(\pm 0.25)$, $R^2=0.991$ for bare NF; $y=11.92(\pm 0.24)\ x+2.071(\pm 0.32)$, $R^2=0.995$ for Ni_3S_2–Et; $y=16.46(\pm 0.37)\ x+1.489(\pm 0.43)$, $R^2=0.999$ for Ni_3S_2–Et/W; $y=14.47(\pm 0.34)\ x+1.618(\pm 0.30)$, $R^2=0.995$ for Ni_3S_2–W.

The Ni_3S_2–Et/W electrode demonstrated excellent linearity between the steady state current and the glucose concentration in the range from 0.0005 to 3 mM, with a high sensitivity of 16,460 $\mu AmM^{-1}cm^{-2}$ (RSD=1.1%), a low detection limit of 0.82 μM, and a low quantification limit of 2.73 μM (Shribasatava et al., 2011). Generally, the blood glucose range is 1.1-20.8 mM for diabetic patients (Wang et al., 2008). For a small amount glucose sensing in urine, saliva, sweat, and food, the sensitivity of prepared electrode was tested in the lower blood glucose range (Wang et al., 2008).

The quantitative results of amperometric responses for the electrodes are summarized in Table S2. As expected from the morphology, electroactive surface area, and electrochemical properties, the hierarchical structure of the Ni_3S_2-Et/W electrode produced high sensitivity and a low detection limit for glucose sensing.

The common existing interferences of human blood serum were investigated to test the selectivity of the Ni_3S_2–Et/W electrode. Figure 5C illustrates the amperometric response of the optimized Ni_3S_2-Et/W electrode to 200 μM of glucose and 10 μM of different interferent

species (fructose, lactose, dopamine, uric acid, and ascorbic acid). Interfering species usually exist with glucose in human blood serum (Yang et al., 2016). The Ni_3S_2–Et/W electrode exhibits a specific response to glucose and a negligible response to these interfering species.

A comparison of the representative non-enzymatic glucose sensors is listed in Table 1. A higher electrochemical performance is presented in order of 3D porous Ni networks on SPCE (Niu et al., 2013), Ni_3S_2 nanosheet arrays on Ni foam (Huo et al., 2014), Ni_3S_2/MWCNT on Ni foam (Radhakrishnan et al., 2015), and NiS on an ITO electrode (Kannan et al., 2015). Nickel sulfide and nickel oxide/hydroxide have similar activities for glucose detection due to similar activity in redox chemistry. Compared with the previous reported electrodes, the Ni_3S_2-Et/W electrode showed a higher sensitivity, low detection limit, and shorter response time.

3.4 Stability and reproducibility

Stability and reproducibility are other critical factors when the material is used in a non-enzymatic glucose sensor. A series of five determinations of 1 mM glucose in 0.5 M NaOH was performed in order to demonstrate the reproducibility of the developed Ni_3S_2-Et/W sensor (RSD=8.6 %). To confirm the long-term stability of the prepared Ni_3S_2-Et/W electrode, an amperometric study was performed in 1 mM glucose/0.5 M NaOH over one month. The prepared electrode was stored at room temperature and tested every five days. The current response toward 1 mM glucose retained 98.9 % of the initial value. The results in Figure 5D show no significant changes in current response over one month. Based on these findings, the Ni_3S_2-Et/W sensor had effective reproducibility and satisfactory stability for use in glucose sensing applications.

3.5 Real sample analysis

To further address the possible selectivity and reliability of the prepared Ni_3S_2-Et/W electrode, human serum samples with known glucose concentrations were analyzed. In Table S3, Sample No. 1 is the original serum (4.89 mM, H4822), purchased from Sigma-Aldrich, and No. 2 and No. 3 were diluted with 0.5 M NaOH solution. The electrochemical detection of glucose using the nickel sulfide electrode was assessed by comparing the amperometric responses from the samples before and after spiking with a standard amount of glucose (5 mM). The results are shown in Table S1, demonstrating spike recoveries of glucose from 92 to 95 %, with RSD of less than 8% from three independent measurements. We conclude that the developed sensor can be used to detect glucose in human samples with sufficient reliability.

4. Conclusion

We demonstrated the varied morphology of Ni_3S_2 fabricated directly on Ni foam through the use of eco-friendly solvent assistance. The morphology was simply controlled by the volume ratio between ethanol and water. The hierarchical cauliflower-like Ni_3S_2 prepared in ethanol and water (1:1) served as an excellent electrode material for glucose sensing. This material achieved a remarkable glucose sensitivity of 16,640 $\mu AmM^{-1}cm^{-2}$ and a low detection limit of 0.82 μM. This result is attributed to the large electroactive surface area and effective ion/electron transfer resulting from the hierarchical structure. Moreover, nickel sulfide electrodes can be useful for use in glucose detection devices, as well as in other electrochemical applications.

Acknowledgment

This study was supported by the Energy Efficiency & Resources of the Korea Institute of Energy Technology Evaluation and Planning (KETEP) grant funded by the Korea government Ministry of Knowledge Economy (No. 20142010102690).

References

Bojdi, M.K, Zadeh M.H.M., Behbahani, M., Farahani A., Davarani S.S.H., Bagheri, A., 2014.Electrochim. Acta 136, 59-65.

Cao, F., Guo, S., Ma, H., Shan, D., Yang, S., Gong, J., 2011.Biosens. Bioelectron. 26, 2756-2760.

Chou, S.-L., Wang, J.-Z., Liu, H.-K., Dou, S.-X., 2008.J. Power Sources 182(1), 359-364.

Chou, S.-W., Lin, J.-Y., 2013. J. Electrochem. Soc. 160(4), D178-D182.

Chou, S.-W., Lin, J.-Y., 2015. J. Electrochem. Soc. 162(14), A2762-A2769.

Cong, H.-P., Yu, S.-H., 2009.Cryst. Growth Des. 9(1), 210-217.

Ghosh, D., Das, C.K., 2015. ACS Appl. Mater.Interfaces 7(2), 1122-1131.

Guo, C., Wang, Y., Zhao, Y., Xu, C., 2013.Anal. Methods 5(7), 1644.

Guo, M.-m., Yin, X.-l., Zhou, C.-h., Xia, Y., Huang, W., Li, Z., 2014.Electrochim. Acta 142, 351-358.

Hosseini,H., Behbahani,M., Mahyari,M., Kazerooni, H., Bagheri, A., Shaabani, A., 2014.Biosens. Bioelectron. 59, 412-417.

Huo, H., Zhao, Y., Xu, C., 2014.J. Mater. Chem. A 2(36), 15111.

Jung, H., Lee, S.H., Yang, J., Cho, M., Lee, Y., 2014.RSC Adv. 4(88), 47714-47720.

Kannan, P.K., Rout, C.S., 2015.Chem. Eur. J 21(26), 9355-9359.

Lee, C.W., Seo, S.D., Park, H.K., Park, S., Song, H.J., Kim, D.W., Hong, K.S., 2015a.Nanoscale 7(6), 2790-2796.

Lee, S.H., Lee, H., Cho, M., Lee, Y., 2015b.Chem. Commun. 51(16), 3391-3394.

Lee, S.H., Lee, H., Cho, M.S., Nam, J.-D., Lee, Y., 2013.J. Mater. Chem. A 1(46), 14606-14611.

Li, D., Li, X., Hou, X., Sun, X., Liu, B., He, D., 2014. Chem. Commun. 50(66), 9361-9364.

Lin, T.W., Dai, C.S., Hung, K.C., 2014a.Sci. Rep. 4, 7274.

Lin, T.W., Liu, C.J., Dai, C.S., 2014b.Appl. Catal., B 154–155, 213-220.

Lu, P., Lei, Y., Lu, S., Wang, Q., Liu, Q., 2015.Anal. Chim. Acta 880, 42-51.

Metcalf, P.A., Fanwick, P., Kąkol, Z., Honig, J.M., 1993.J. Solid State Chem. 104(1), 81-87.

Niu, X., Lan, M., Zhao, H., Chen, C., 2013.Anal. Chem. 85(7), 3561-3569.

Qian, L., Mao, J., Tian, X., Yuan, H., Xiao, D., 2013.Sens. Actuators, B 176, 952-959.

Radhakrishnan, S., Kim, S.J., 2015.RSC Adv. 5(55), 44346-44352.
Shen, X.W., Huang, C.Z., Li, Y.F., 2007.Talanta 72, 1432-1437.
Shribasatava A., Gupta V. B., 2011. CHRON. YOUNG SCI. 2, 21-25
Wang, G., Lu, X., Zhai, T., Ling, Y., Wang, H., Tong, Y., Li, Y., 2012.Nanoscale 4(10), 3123-3127.
Wang, J. 2008 Chem. Rev. 108, 814-825.
Wang, J., Chao, D., Liu, J., Li, L., Lai, L., Lin, J., Shen, Z., 2014.Nano Energy 7, 151-160.
Wang, Q., Wen, Z., Li, J., 2006a.Inorg Chem 45(17), 6944-6949.
Wang, Q., Gao, R., Li, J., 2007.Appl. Phys. Lett. 90, 143107
Wang, W., Wang, S.-Y., Gao, Y.-L., Wang, K.-Y., Liu, M., 2006b.Mater. Sci. Eng., B 133(1–3), 167-171.
Wang, W., Zhang, L., Tong, S., Li, X., Song, W., 2009.Biosens. Bioelectron. 25, 708-714.
Yang, J., Cho, M., Lee, Y., 2016.Sens. Actuators, B 222, 674-681.
Yang, Y., Yu, J.H., Strickler, J.R., Chang, W.J., Gunasekaran. S., 2013.Biosens. Bioelectron. 47, 530-538.
Yu, S.H., Yoshimura, M., 2002.Adv. Funct. Mater. 12(4), 277-285.
Zhang, J., Sun, Yin, Su, Liao, Yan, 2002.Chem. Mater. 14(10), 4172-4177.
Zhang, L., Yu, J.C., Mo, M., Wu, L., Li, Q., Kwong, K.W., 2004.J. Am. Chem. Soc. 126(26), 8116-8117.
Zhang, X., Wang, G., Gu, A., Wei, Y., Fang, B., 2008.Chem. Commun. (45), 5945-5947.
Zhang, Y., Wang, Y., Jia, J., Wang, J., 2012.Sens. Actuators, B 171-172, 580-587.
Zhang, Z., Huang, Z., Ren, L., Shen, Y., Qi, X., Zhong, J., 2014.Electrochim. Acta 149, 316-323.
Zhao, Y., Gu, G., You, S., Ji, R., Suo, H., Zhao, C., Liu, F., 2015.RSC Adv. 5(66), 53665-53670.
Zhou, W., Chen, W., Nai, J., Yin, P., Chen, C., Guo, L., 2010.Adv. Funct. Mater. 20(21), 3678-3683.
Zhou, W., Wu, X.-J., Cao, X., Huang, X., Tan, C., Tian, J., Liu, H., Wang, J., Zhang, H., 2013.Energy Environ Sci 6(10), 2921.

Figure 1. Schematic representation of preparation of nickel sulfide on Ni foam as a reactive substance according to the volume ratio between ethanol and water

Figure 2. SEM images of nickel sulfide using various reaction medium: Ni_3S_2–Et (A), Ni_3S_2–Et/W (B), Ni_3S_2–Et/W with high magnification (C), and Ni_3S_2–W (D), and

EDS maps of nickel, sulfur, and oxygen from Ni_3S_2–Et/W (E)

Figure 3. (A) XRD pattern of the nickel sulfides: Ni_3S_2–Et, Ni_3S_2 –Et/W, and Ni_3S_2 –W. (B) XRD diffraction peak of Ni_3S_2–Et/W. XPS profiles of as-prepared Ni_3S_2–Et/W electrode: full scan (C); Ni (D); and S (E)

Figure 4. (A) Nyquist plots of bare Ni foam (a), Ni_3S_2–Et (b), Ni_3S_2–Et/W (c), and Ni_3S_2–W (d) in 0.1 M KCl containing 1 mM $Fe(CN)_6$. (B) CVs of various electrodes in 0.5 M NaOH solution at 10 mVs^{-1}. (C) CVs with different scanning rates of Ni_3S_2–Et/W from 5 to 100 mVs^{-1}. (D) Redox peak currents obtained from Fig 4C as a function of the square root of the scanning rates (E) CVs in 1 mM glucose/0.5 M NaOH aqueous solution at 20 mVs^{-1}.

Figure 5. (A) Amperometric response of bare NF (a), Ni_3S_2–Et (b), Ni_3S_2–Et/W (c), and Ni_3S_2–W (d) in 0.5 M NaOH with stepwise addition of glucose (0.5, 10, 100, 200 and 400 μM, respectively) stock solution at applied potential, +0.55 V. Inset: magnification of curve c. (B) Calibration curves of current response vs. glucose concentration from Fig 5A. (C) Amperometric response of Ni_3S_2–Et/W in successive addition of 200 μM Glucose and 10 μM interferences (Fructose, Lactose, AA, DA, and UA) in 0.5 M NaOH at applied potential: +0.55 V. (D) Retention percentage of initial response of Ni_3S_2–Et/W sensor to 1 mM glucose tested by amperometric measurements over one month.

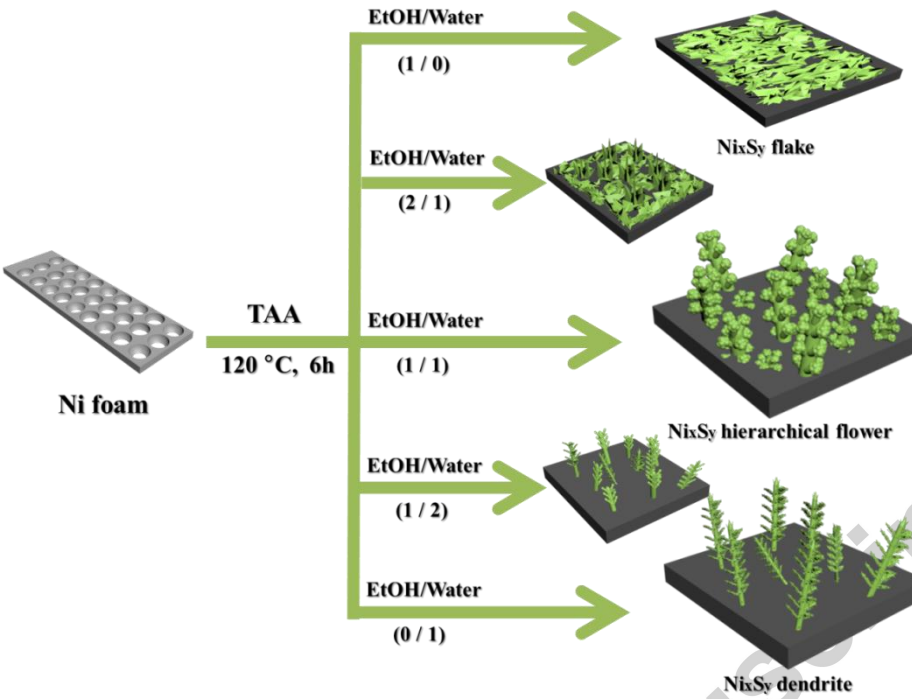

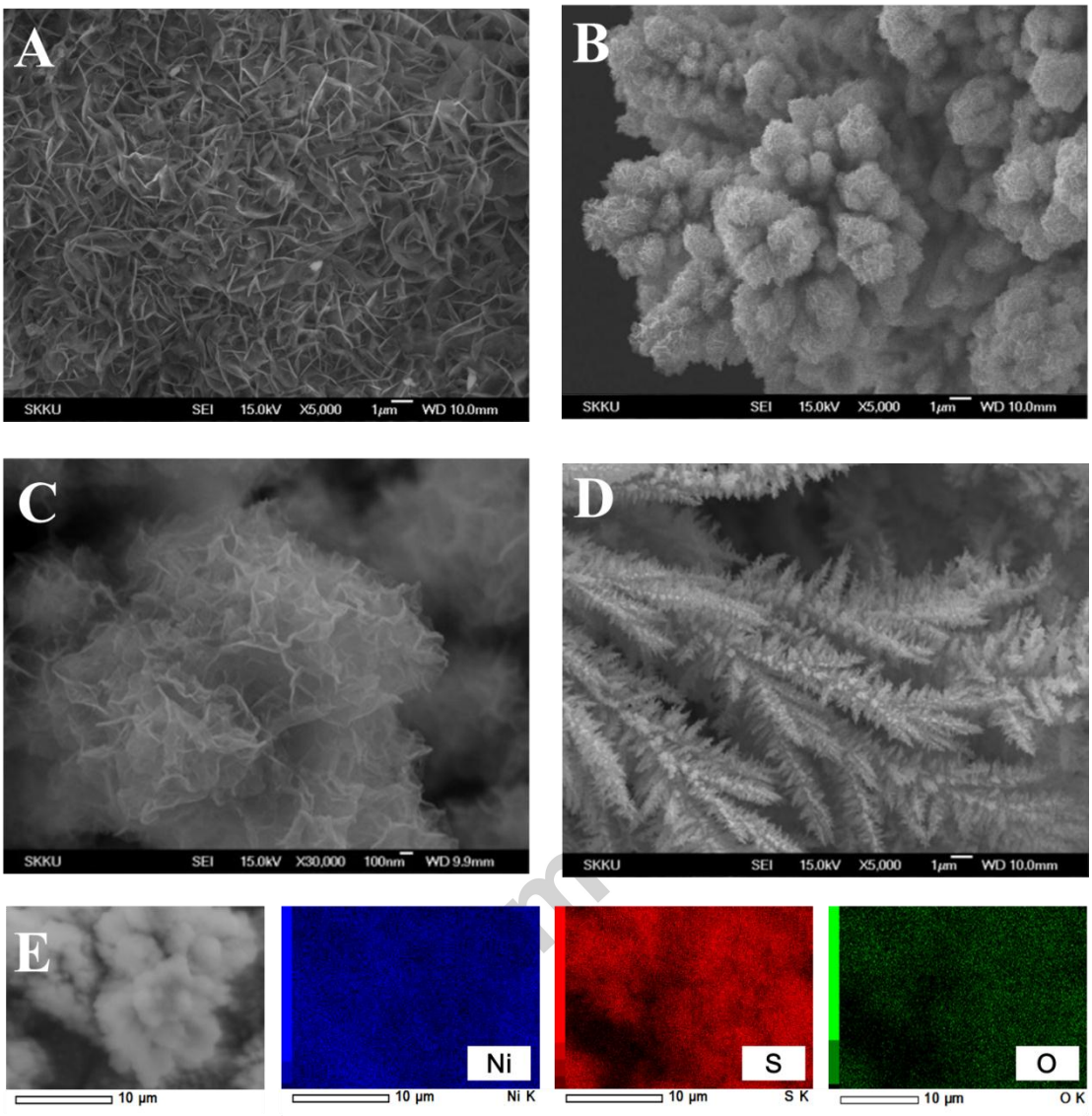
A
SKKU SEI 15.0kV X5,000 1μm WD 10.0mm
B
SKKU SEI 15.0kV X5,000 1μm WD 10.0mm
C
SKKU SEI 15.0kV X30,000 100nm WD 9.9mm
D
SKKU SEI 15.0kV X5,000 1μm WD 10.0mm
E
10 μm
Ni
10 μm Ni K
S
10 μm S K
O
10 μm O K

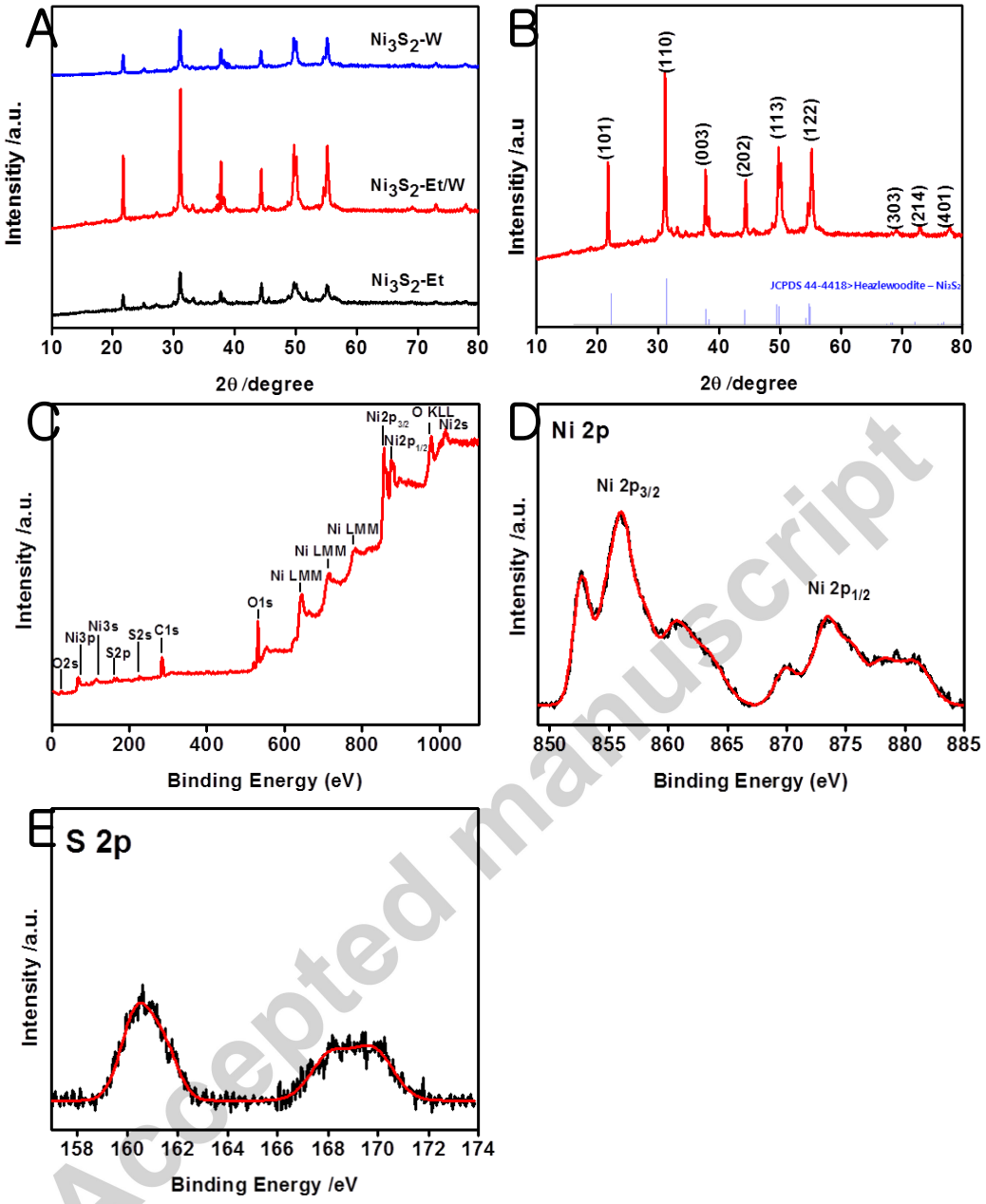

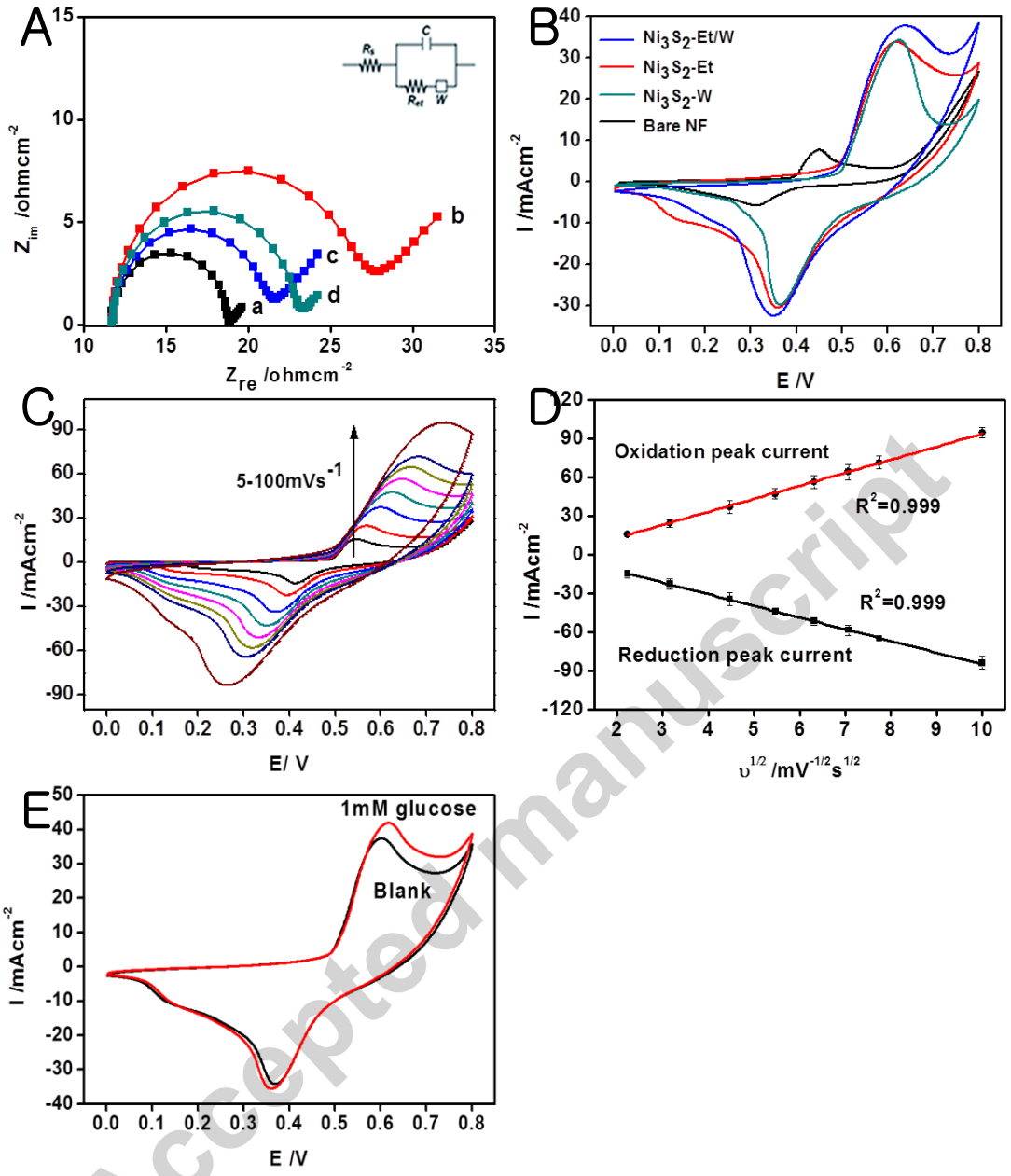

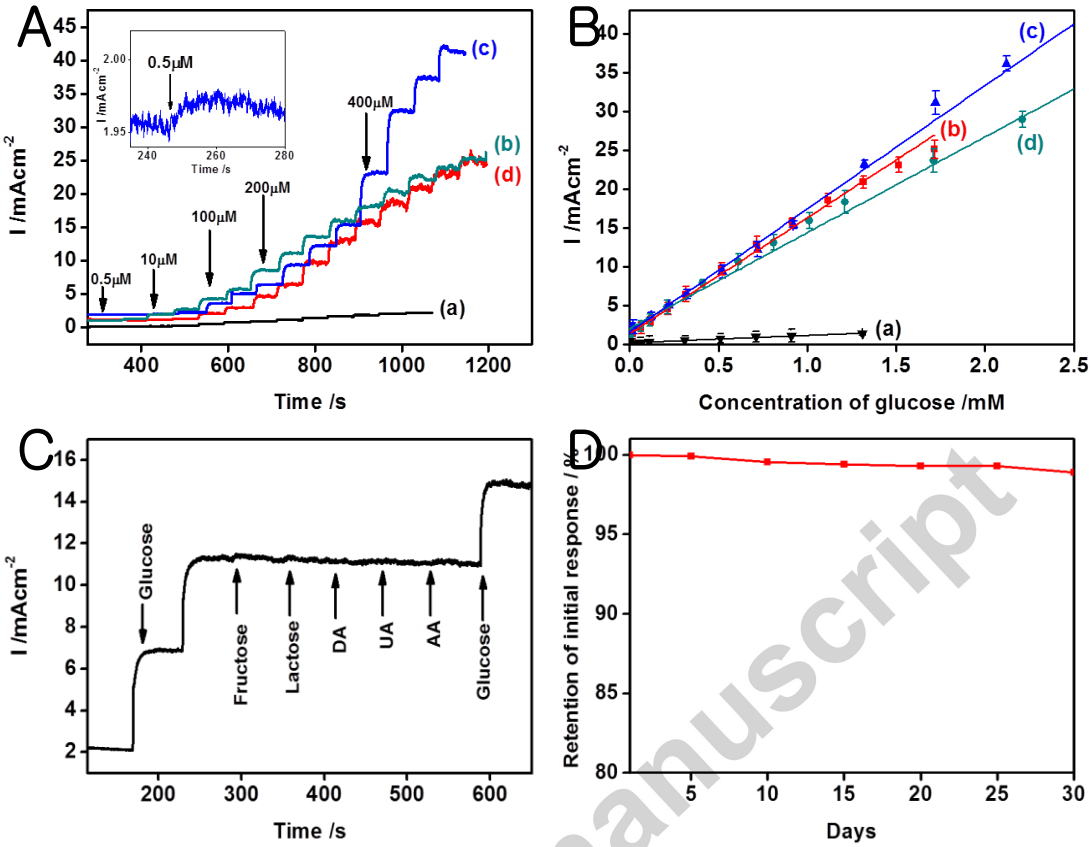

Table 1. Comparison of glucose sensing performance of nickel sulfides with some reported sensors

Electrode	Sensitivity ($\mu AmM^{-1}cm^{-2}$)	Linear Range (mM)	Low detection limit (μM)	Ref.
CuS nanotube/Cu	3,135	0.0002-2.5	0.045	Qian et al., 2013
$Ni(OH)_2$/gold	3,529	0.002-7	0.73	Guo et al., 2014
Ni/NiO/Cu	4,490	0.01-8.3	-	Zhang et al., 2012
NiO nano flake arrays/FTO	8,500	0.01-0.8	1.2	Wang et al., 2012
3D porous Ni/SPCE[a]	2,900	0.0005-4	0.07	Niu et al., 2013
NiO/NF[b]	6,657	0.005-5.5	0.46	Guo et al., 2013
NiS/RGO/GCE	-	0.00005-1.7	0.1	Radhakrishnan et al., 2015
NiS/ITO	7,430	0.005-0.045	0.32	Kannan et al., 2015
Ni_3S_2/MWCNT/NF	3,345 μAmM^{-1}	0.03-0.5	1.0	Lin et al., 2014b
Ni_3S_2 nanosheet/NF	6,148	0.005-3.0	1.2	Huo et al., 2014
Ni_3S_2 hierarchical nano cauliflower/NF	16,460	0.0005-3.0	0.82	This work

[a] SPCE: Screen-printed carbon electrode, [b] NF: Nickel foam

Highlights

- This paper analyses glucose based on nickel sulphides prepared by solvent assist.
- The hierarchical cauliflower-like structure is obtained in ethanol and water co-solvent.
- The sensor shows high sensitivity (16,460 $\mu A\ mM^{-1}cm^{-2}$) and high

selectivity.